Proceedings of the 11th ICPMG 2026
11th International Conference on Physical Modelling in Geotechnics
8-12 June 2026, Zurich, Switzerland

Effect of relative density on repeated liquefaction behavior using centrifuge modelling

J. Florez
Kyoto University, Uji, Japan, florez.jhon.28s@st.kyoto-u.ac.jp

N. Takamatsu, K. Ueda and R. Uzuoka
Disaster Prevention Research Institute, Kyoto University, Uji, Japan,
takamatsu.nao.76v@st.kyoto-u.ac.jp ueda.kyohei.2v@kyoto-u.ac.jp uzuoka.ryosuke.6z@kyoto-u.ac.jp

ABSTRACT: Repeated liquefaction occurs when a soil experiences multiple liquefaction events due to successive seismic loadings, with the excess pore water pressure required to fully dissipate after each shaking episode. Although previous studies have reported changes in soil resistance following an initial liquefaction event, the influence of relative density on this behavior remains insufficiently understood. This study investigates the effect of relative density on the repeated liquefaction response of sandy soils using centrifuge modelling. Experiments were conducted under a centrifugal acceleration of 50g to replicate prototype stress conditions. The results demonstrate that while loose specimens (Dr=50%) exhibit post-shaking strength recovery at greater depths due to densification, dense specimens (Dr=80%) show a continuous reduction in cone resistance across the profile.

1 INTRODUCTION

Multiple factors, such as input motion characteristics, pre-shaking history, liquefaction history, microstructural anisotropy, soil gradation, and geologic age, have been identified as key influences on the liquefaction and repeated liquefaction potential of sands (Oda et al., 2001). Field observations indicate that sites with a prior liquefaction history (hereafter post-liquefied sites) tend to exhibit increased susceptibility to liquefaction during subsequent earthquakes. This behavior has been documented in several events, such as the 1983 Nihonkai–Chubu Earthquake (Yasuda & Tohno, 1988) and the 2011 Great East Japan Earthquake (Yasuda et al., 2012). In the present study, relative density is considered the primary variable of interest. A series of centrifuge experiments were performed to evaluate differences in soil response at two relative densities. The comparison focuses on (1) CPT profiles obtained before and after the first shaking event and (2) the soil response, specifically acceleration and pore water pressure, recorded during the first and second shaking events.

2 EXPERIMENTAL PROCEDURE

2.1 Centrifuge facility

The centrifuge experiments were conducted at the Disaster Prevention Research Institute (DPRI), Kyoto University. Table 1 outlines the technical specifications of the centrifuge machine used.

Table 1. Technical Specifications of the Centrifuge Machine

Parameter	Value
Effective radius	2.5 m
Max payload	24 g-ton
Maximum centrifugal acceleration	200 g
Maximum number of rotations	260 rpm
Maximum payload at 50g	Dynamic:142.5 kg

A rigid container with internal dimensions of 450 mm × 150 mm × 300 mm (length × width × height) was employed for the experiments. Fig. 1 shows the rigid container securely mounted within the centrifuge chamber before testing.

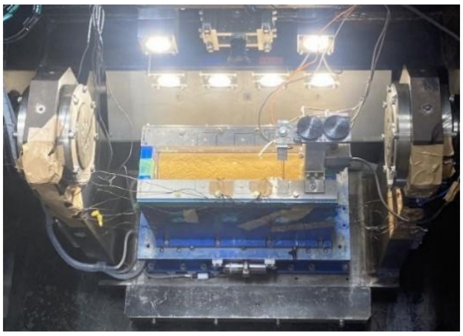

Figure 1. Experimental setup.

2.2 Scaling laws

The experiment was conducted under a centrifugal acceleration of 50g, and the findings are reported in terms of equivalent prototype units, unless specified. To facilitate the conversion from model scale to prototype scale, the scaling factors employed are detailed in Table 2. These factors are crucial for accurately interpreting the results and ensuring that the model's behavior is representative of the actual prototype. By using these scaling factors, we can draw meaningful conclusions about the performance and characteristics of the prototype based on the model's behavior under controlled conditions.

Table 2. Scaling factors for common parameters (Kutter, 1994)

Parameter	Ratio of model to prototype (a)
Length	$1/n$
Area	$1/n^2$
Volume	$1/n^3$
Stress	1
Strain	1
Force	$1/n^2$
Velocity	1
Acceleration	n
Frequency	n
Time (dynamic)	$1/n$
Time (consolidation)	$1/n^2$

(a) n = centrifuge acceleration
(b) Consolidation time scaling based on same pore fluid in model and prototype.

2.3 Sample preparation and instrumentation

For this study, Japanese Toyoura Sand was selected due to its uniform particle size distribution and well-documented geotechnical properties (see Table 3). Toyoura Sand consists predominantly of sub-rounded to subangular particles, with a mineral composition of approximately 75% quartz, 22% feldspar, and 3% magnetite (Oda et al., 1978).

Table 3. Characteristics for Toyoura sand (Uemura, 2010).

Parameter	Symbol	Value
Grain size, 50 %	d_{50}	0.171 mm
Specific gravity	G_s	2.635
Maximum void ratio	e_{max}	0.991
Minimum void ratio	e_{min}	0.624

Soil specimens were prepared using the air pluviation method to achieve relative densities of 50% and 80%. The sensor distribution is displayed in Fig. 2.

It is well recognized that rigid boundaries can induce wave reflections that may affect the soil response near the container walls. To mitigate these boundary effects, the instrumentation was strategically concentrated within the central region of the model (the middle 40% of the container length). Previous studies on boundary effects in centrifuge modelling (Coelho et al., 2003) have indicated that while boundaries significantly influence the response at the edges, the soil behavior observed in the model's center remains authentic and representative. Therefore, this study focuses exclusively on the response of this central zone, and no sensors were placed in the boundary-affected regions.

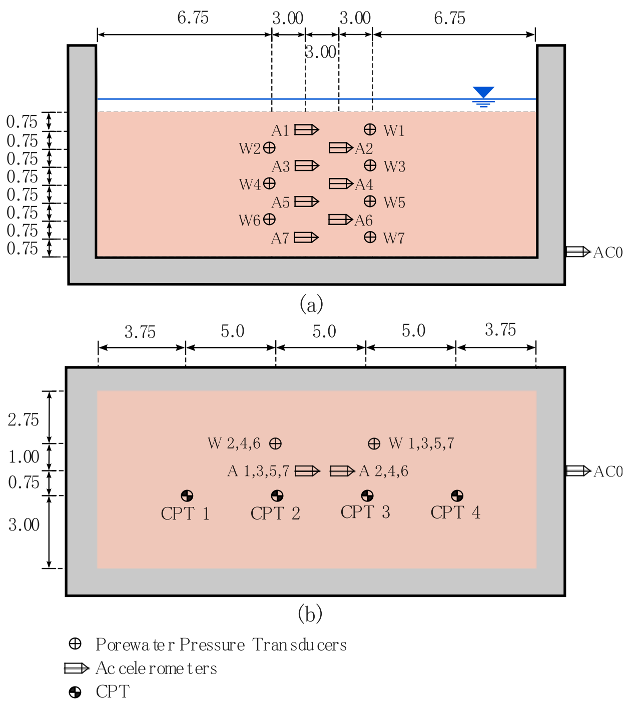

Figure 2. Soil Configuration (a) Side View (b) Top View. All dimensions are expressed in meters.

Details of the CPT device used in this research are provided in Carey (2018). The original model was slightly modified for the present study by removing all O-rings except the one located near the cone tip, in order to minimize contact between the rod and the sleeve. The applied corrections and further details of the implications of this modification are described in a later section

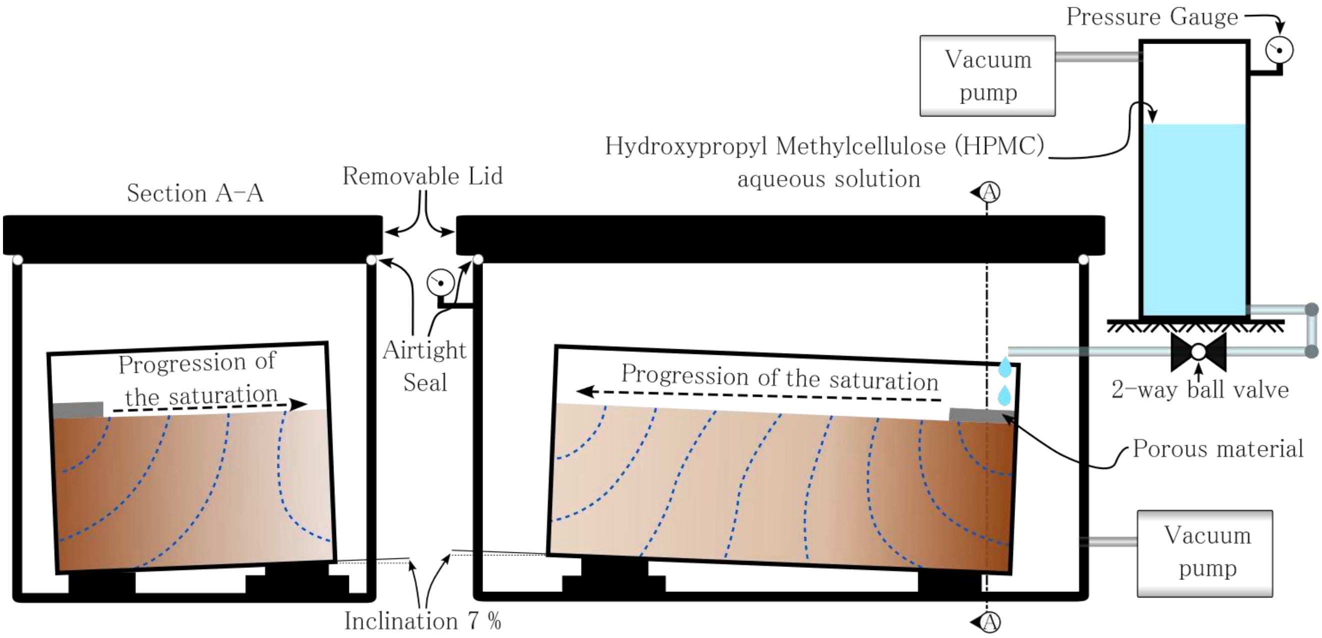

Figure 3. Schematic layout of the experimental setup for the vacuum de-airing process of the HPMC pore fluid and the saturation of the soil model.

To satisfy the scaling laws and ensure that excess pore water pressure can properly build up without dissipating prematurely, an aqueous solution of Hydroxypropyl Methylcellulose (HPMC) was employed as the pore fluid, calibrated to a target kinematic viscosity of 50 cSt. The solution was pre-mixed in a separate container until the target viscosity was achieved and verified. Once prepared, the fluid was transferred to the de-airing tank shown in Fig. 3 to undergo a thorough vacuum process, ensuring fluid incompressibility and accurate pore pressure generation during the experiment. During the saturation stage, a porous material (sponge) was placed on the sand surface to protect the soil fabric from the impact of fluid dropping from, thereby preserving the initial relative density. Furthermore, the model container was subjected to a dual-axis inclination of 7% (tilted along both its longitudinal and transverse axes). This compound tilting ensured that only a single bottom corner remained at the lowest gravitational point, facilitating a controlled, upward diagonal saturation front that effectively eliminated the likelihood of trapping air pockets within the soil matrix.

2.4 Seismic excitation

The horizontal input motion was one-dimensional, featuring multiple cycles at a frequency of 1 Hz with a duration of 30 seconds. The PGA for both events was nearly 2.5 m/s2 (see Fig. 4). The loading was divided into two distinct phases:

- Linearly increasing: Gradual ramp-up of accelerations to the target peak value.
- Linearly decreasing: Gradual ramp down of acceleration to zero.

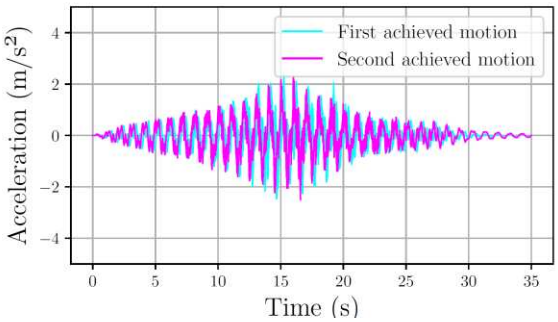

Figure 4. Achieved model container motion for first and second shaking. Procedure B, 80% (similar achieved waves were recorded for the other experiments).

2.5 Centrifuge procedure

Two testing procedures were adopted in this study, differing in the sequence of CPT measurements and shaking events:

- Procedure A: Four CPTs were performed first, followed by the application of two shaking events.
- Procedure B: A first shaking event was applied before conducting the four CPTs, and the second shaking event was applied afterward.

These procedures were specifically designed to evaluate the changes in cone tip resistance (qc) following an initial shaking event, while ensuring reliable pre- and post-shaking soil characterization.

The motivation for performing four CPTs prior to the first shaking event (in Procedure A) was to obtain multiple measurements at different locations within the model. This approach allows assessment of the repeatability and spatial variability of the initial soil conditions.

However, each CPT penetration disturbs the surrounding soil within an affected zone estimated. To avoid potential interference or influence from previous penetrations on subsequent measurements, particularly for post-shaking CPTs, a separate identical model was prepared and tested under the same conditions. This second model was used exclusively for conducting the four CPTs after the shaking events, ensuring that the post-liquefaction soil state could be characterized without significant disturbance effects from prior penetrations.

A summary of the overall testing sequence for both procedures is presented in Fig. 5. The following nomenclature will be used to refer to each experiment presented in the results: the first letter corresponds to the applied procedure, the following two numerical digits indicate the relative density of the soil, and the final letter denotes the shaking event number. For example, B50F represents procedure B, a relative density of Dr = 50% and the first shaking event.

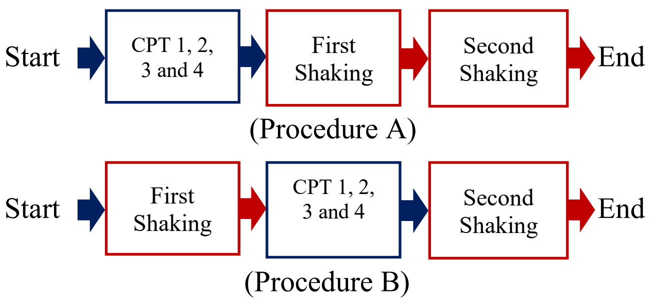

Figure 5. Centrifuge Experiment procedures.

In prototype scale, the container plan dimensions are 22.5 m × 7.5 m, corresponding to approximately 75 and 25 cone diameters, respectively, for a cone diameter of 0.3 m. Previous centrifuge studies (Darby et al., 2019) indicate that cone penetration influences the surrounding soil within approximately 5–10 times the cone diameter (d_c). In the present tests, the distances from the center of the CPT to the accelerometers and pore pressure transducers are approximately 1.25 m (≈ 4.2 d_c) and 2.66 m (≈ 8.9 d_c), respectively. Therefore, the pore pressure sensors are located well outside the zone of strongest CPT influence, and the accelerometers are at the lower bound of this range. Moreover, the potentially disturbed zone represents only a small fraction of the overall model dimensions, indicating that the recorded dynamic response is governed by the global soil behavior rather than by localized CPT-induced disturbance. Nevertheless, the absence of a dedicated control test without intermediate CPTs is acknowledged as a limitation of the study.

3 TEST RESULTS

Figures 10 and 11 illustrate the soil response for models with relative densities of Dr = 50% and Dr = 80%, respectively. These figures show the acceleration response and evolution of excess pore water pressure (EPWP) during the shaking events.

3.1 Porewater pressure response

The pore pressure ratio (r_u) was estimated to evaluate the occurrence of liquefaction in the soil model. Liquefaction is considered to have occurred when the r_u value is equal to or close to 1. The $r_u = 1$ was calculated by dividing the porewater pressure generated during shaking events at a specific depth by the initial vertical effective stress at the same depth.

In test B50F, sensors W1, W2, W3, and W4 reached r_u values of 1, indicating that liquefaction occurred at these locations. The start time, end time, and total duration of liquefaction for each sensor are summarized in Figure 6. It is observed that sensors W1 and W2 exhibit the longest liquefaction durations; however, at sensor W1, liquefaction starts after the seismic shaking has finished (after 30 s). This behavior is attributed to post-shaking pore water pressure redistribution. The upward flow generated during the dissipation of excess pore water pressure from deeper regions creates a hydraulic gradient that continues to reduce the effective stress at shallow depths, eventually triggering liquefaction even in the absence of cyclic loading.

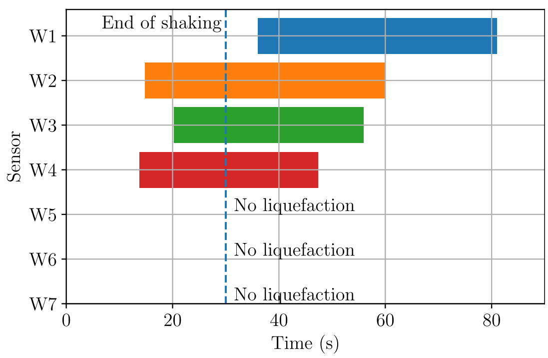

Figure 6. Liquefaction timeline for test B50F. Horizontal bars indicate the onset and duration of liquefaction at each pore pressure sensor. The vertical dashed line marks the end of seismic shaking

In the second shaking event of the model with Dr = 50% (B50S), liquefaction developed mainly at sensors W1, W2, and W3 (see Figure 7). In this test, the duration of liquefaction was shorter than in the first event, which is consistent with the progressive improvement of the soil following the initial shaking.

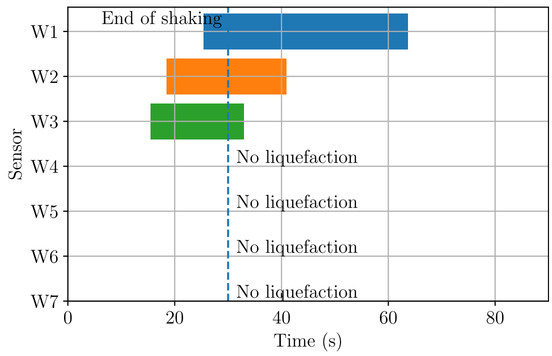

Figure 7. Liquefaction timeline for test B50S. Horizontal bars indicate the onset and duration of liquefaction.

For the models with relative density Dr = 80%, the soil response differed significantly. In test B80F(see Figure 8), liquefaction durations were shorter than those in the Dr = 50% tests. Notably, sensor W3 exhibited a delayed onset of liquefaction, reaching $r_u = 1$ only after the cessation of seismic shaking. This delay is attributed to a combination of spatial pressure distribution and the dilative nature of dense sand.

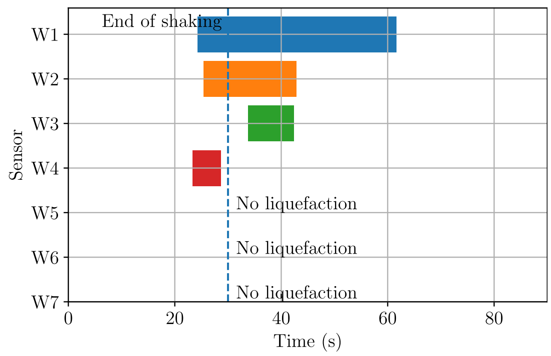

Figure 8. Liquefaction timeline for test B80F. Horizontal bars indicate the onset and duration of liquefaction.

In this experimental setup, odd-numbered sensors (including W1 and W3) were located 4.5 m (prototype scale) to the right of the center, while even-numbered sensors were on the left. The recorded data indicates a slightly slower rate of pore pressure generation on the right side of the model. For the shallowest sensor, W1, the low initial effective stress allowed liquefaction to be triggered relatively quickly despite this asymmetry.

In the second shaking event with Dr = 80% (see Figure 9), liquefaction was even more limited than in B80F. It was only observed at sensor W1 and persisted for a relatively short time.

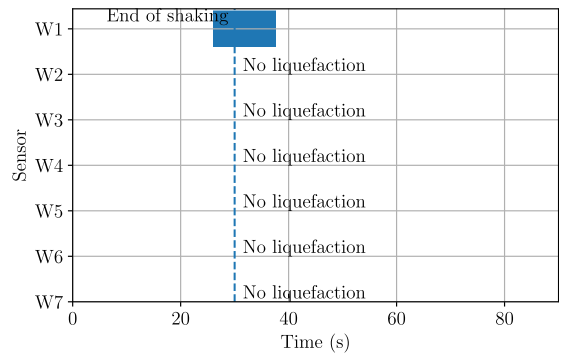

Figure 9. Liquefaction timeline for test B80S. Horizontal bars indicate the onset and duration.

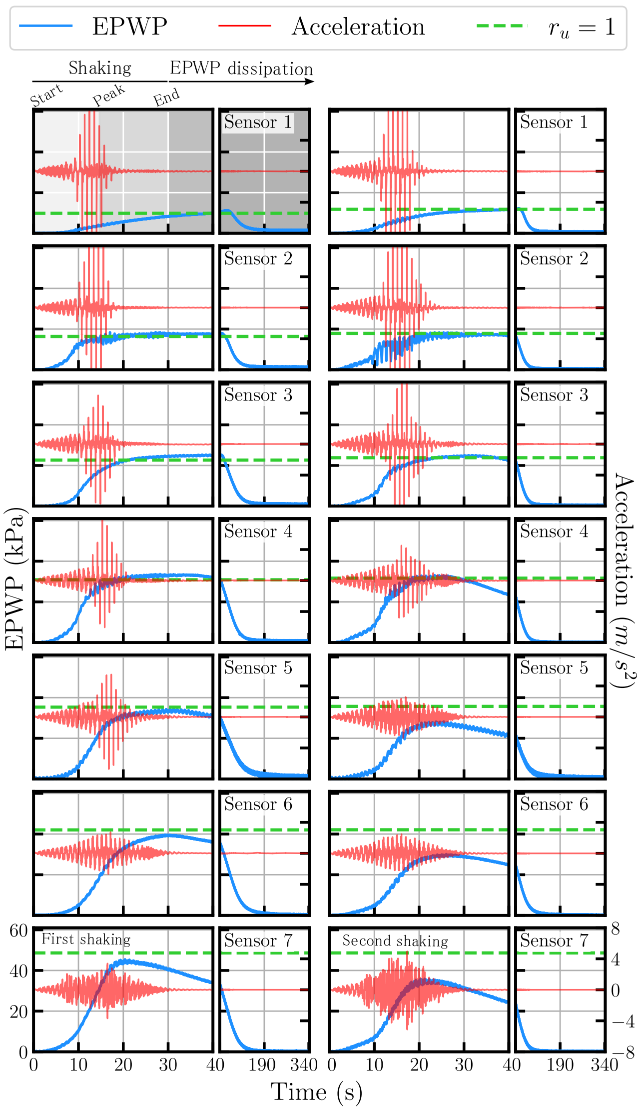

Figure 10. Soil response during shaking (Dr = 50%, Procedure B). Left: first shaking; right: second shaking.

3.2 Acceleration response

Acceleration response from A1 (sensor 1) to A7 (sensor 7) for B50F and B50S are shown in Fig. 10. The recorded acceleration time histories show that the input motion changed as it propagated through the liquefied soil layer. Sharp acceleration pulses were observed during shaking, particularly in the upper part of the deposit.

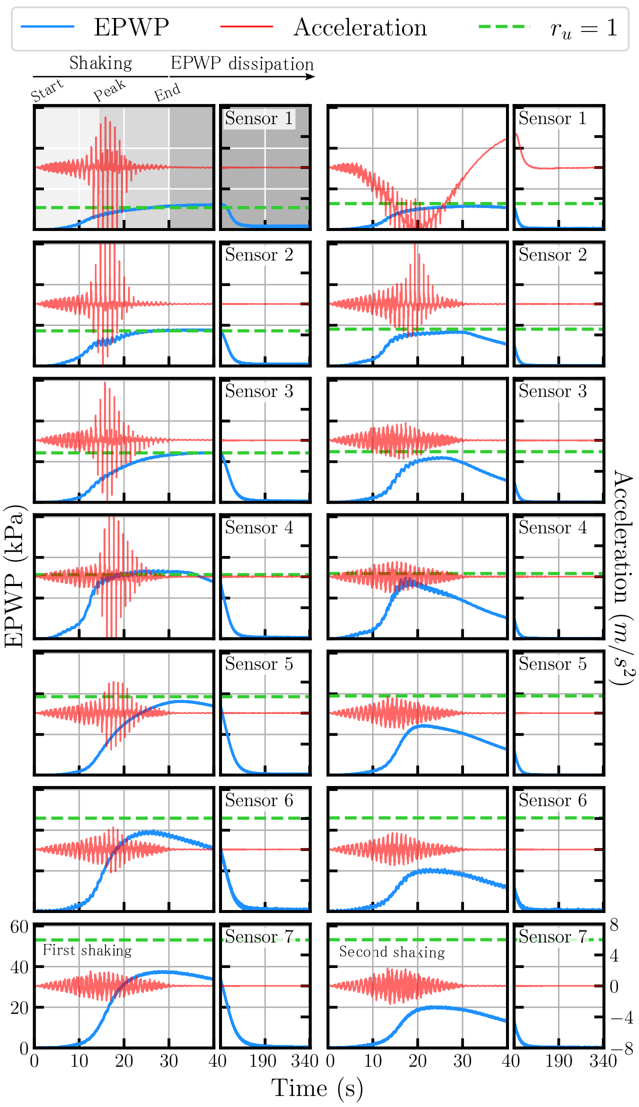

Figure 11. Soil response during shaking (Dr = 80%, Procedure B). Left: first shaking; right: second shaking.

At shallow sensors for B50F, acceleration amplitudes were strongly attenuated once liquefaction was triggered (A1, A2 and A3), indicating a substantial loss of stiffness and an inability of the soil to transmit shear stresses. These observations are consistent with the evolution of excess porewater pressure and indicate that the acceleration response is strongly governed by the interplay between liquefaction and stiffness degradation.

In experiment B50S, A4 and A5 response did not show sharp spikes in comparison to B50F while the time of liquefaction comparing the first and second shaking was shorter in W4 and it did not liquefy in W5.

Acceleration response at A2, A4, A5 and A7 for B80F and B80S is shown in Fig. 11. The recorded acceleration time histories show that the input motion changed less during the second shaking.

3.3 CPT results

For each CPT, the acquisition system records three channels denoted as TimeX, LoadX, and DisplacementX, where X identifies the penetration number.

The physical process observed during the initial penetration is illustrated schematically in Figure 12 and can be divided into three distinct stages:

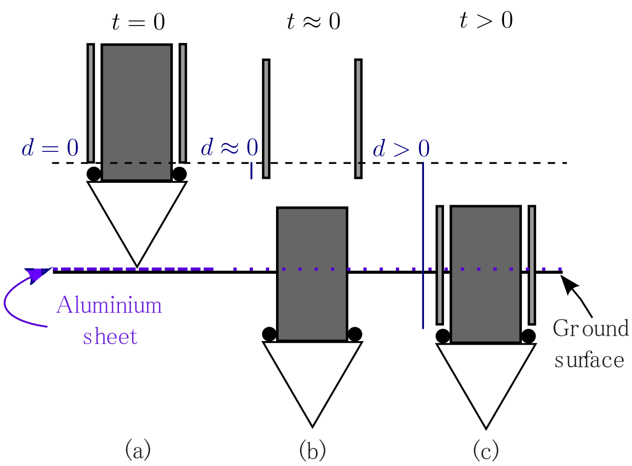

Figure 12. Stages of penetration at achieved gravity (50g) (a) Zero-penetration reference (b) Self-weight-driven penetration (c) Load-cell engagement.

Stage (a): Zero-penetration reference. The cone tip is initially positioned at the ground surface and restrained by an aluminium sheet, which prevents downward movement under self-weight. This configuration defines the true zero-penetration reference, as soil resistance at shallow depths is insufficient to support the weight of the rod–cone.

Stage (b): Self-weight-driven penetration. Once penetration starts, the aluminium sheet ruptures and the rod–cone assembly accelerates downward under its own weight, penetrating faster than the sleeve–load-cell system. This temporary separation results in continued displacement measurements but no valid tip resistance recordings. The motion ends when soil resistance balances the stress induced by the self-weight, allowing the sleeve and load cell to catch up and re-establish contact.

Stage (c): Load-cell engagement. After contact is restored, continuous tip resistance measurements begin. The penetration depth at this stage already includes the displacement accumulated during the self-weight-driven phase and must therefore be corrected using equation 1.

$$q_c^{corr} = q_c^{meas} + q_{rod+tip} \quad (1)$$

where q_c^{meas} is the measured resistance and $q_{rod+tip}$ is the stress associated with the rod-tip self-weight. Subsequently, the corrected $q_c - depth$ curve was back-projected to the origin (0,0) to reconstruct the penetration response during the phase in which no load-cell data were recorded. Several fitting functions were evaluated, and a logarithmic model provided the best match. The data points generated from this logarithmic back-projection were then combined with the corrected experimental measurements.

A limitation of this approach is the possible intrusion of sand into the sleeve during the transition from stages (b) to (c), which may affect load-cell contact conditions. Therefore, four penetrations were performed per experiment, and repeatability was used to identify and discard anomalous measurements.

Figures 13 and 14 present the corrected CPT profiles obtained before and after shaking for specimens prepared at relative densities of Dr=50% and Dr=80% respectively. The post-shaking CPTs were performed after completion of the shaking sequence, and the complete dissipation of the excess pore water pressure.

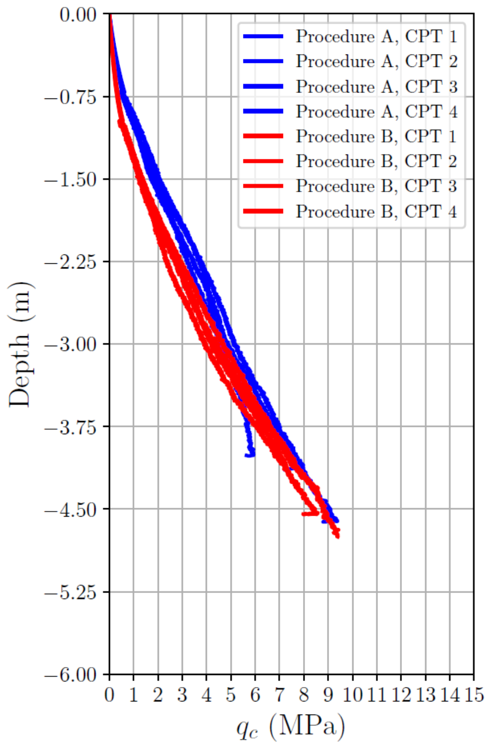

Figure 13. Tip resistance for Dr=50%.

For the specimen with Dr=50%, a clear reduction in cone tip resistance is observed after shaking within the upper portion of the profile, extending from the ground surface to approximately −3.75m. This depth interval coincides with the locations of pore pressure transducers W1 (−0.75m), W2 (−1.50m), W3 (−2.25m), and W4 (−3.00m). The reduction in q_c indicates a degradation of soil strength associated with excess pore pressure generation and loss of effective stress during shaking.

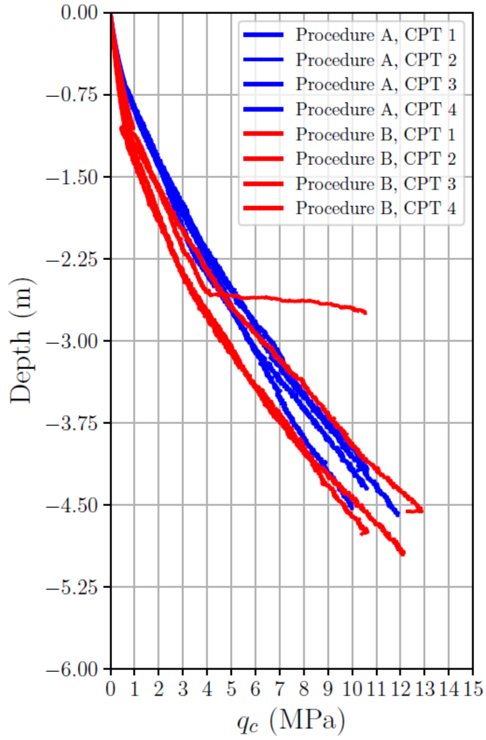

Figure 14. Tip resistance for Dr=80%.

Below this depth, the post-shaking cone resistance gradually increases and becomes comparable to, or slightly exceeds, the pre-shaking values. This behaviour suggests that reconsolidation and post-shaking densification were more effective at greater depths, where confining stresses are higher and excess pore pressure dissipation is more efficient.

In contrast, the specimen prepared at Dr=80% exhibits a more pronounced and continuous reduction in cone tip resistance after shaking, extending from the surface to approximately −4.50m, which corresponds to the maximum penetration depth achieved in the test. Unlike the looser specimen, no clear recovery or increase in q_c is observed within the explored depth range. This indicates that, despite the higher initial density, the denser specimen experienced a more widespread redistribution of soil structure and stiffness during shaking.

It is important to address the apparent contradiction between the reduced liquefaction duration observed in the second shaking events (B50S and B80S) and field observations reported by Yasuda et al. (2012), which suggest that post-liquefied sites often exhibit increased susceptibility to re-liquefaction. This divergence highlights the distinct mechanisms governing laboratory specimens versus field deposits. In the loose model (Dr=50%), the response is dominated by seismic densification (volumetric contraction), leading to an improvement in the soil conditions. Conversely, for the dense model (Dr = 80%), the CPT results (Fig. 14) reveal a reduction in cone tip resistance after shaking, indicating a disruption of the interlocked soil fabric. This "weakening" of the soil structure is consistent with the deleterious effects observed in the field. However, unlike loose field deposits that may re-liquefy due to this structural loss, the absolute density of the Dr=80% specimen remains sufficiently high to suppress full liquefaction during the second event, despite the reduction in stiffness. Thus, the laboratory results isolate the competition between densification and fabric destruction, which manifests differently depending on the initial density state.

4 CONCLUSIONS

The four CPT penetrations performed at A50, B50, and A80, together with two penetrations at B80, yielded similar tip resistance profiles. This consistency demonstrates good repeatability and supports the reliability of the adopted CPT testing and correction approach.

Shaking induced measurable changes in cone tip resistance, particularly within the upper soil layers, indicating a significant modification of the soil response due to seismic loading.

In the looser specimen (Dr = 50%), cone resistance recovers and increases at greater depths, suggesting that reconsolidation effects are more pronounced under higher confining stress, while shallower layers remain more affected by shaking-induced disturbance.

In contrast, the dense specimen (Dr = 80%) exhibited a continuous reduction in cone resistance throughout the explored depth. This indicates that for higher initial densities, the seismic loading primarily induces a widespread redistribution of soil fabric.

We had the occurrence of delayed, post-shaking liquefaction at shallow depths (sensor W1). This behavior is attributed to pore water pressure redistribution (upward flow), demonstrating that liquefaction can be triggered by hydraulic gradients even after the end of seismic loading.

REFERENCES

Carey, T., Gavras, A., Kutter, B. L., Haigh, S. K., Madabhushi, S. P. G., Okamura, M., *et al.* (2018). A new shared miniature cone penetrometer for centrifuge testing. In *Physical Modelling in Geotechnics, Volume 1* (pp. 293–298). CRC Press.

Coelho, P. A. L. F., S. K. Haigh, and S. P. G. Madabhushi (2003). Boundary effects in dynamic centrifuge modelling of liquefaction in sand deposits. Proceedings of the 16th ASCE Engineering Mechanics Conference, Seattle, WA, USA.

Darby, K. M., R. W. Boulanger, J. T. DeJong, and J. D. Bronner (2019). Progressive Changes in Liquefaction and Cone Penetration Resistance across Multiple Shaking Events in Centrifuge Tests. Journal of Geotechnical and Geoenvironmental Engineering, 145(3), 04018112. http://doi.org/10.1061/(ASCE)GT.1943-5606.0001995

Kutter, B. L. (1994). Recent advances in centrifuge modeling of seismic shaking. In *Proceedings of the 3rd International Conference on Recent Advances in Geotechnical Earthquake Engineering and Soil Dynamics* (pp. 927–942). St. Louis, MO.

Oda, M., Kawamoto, K., Suzuki, K., Fujimori, H., & Sato, M. (2001). Microstructural interpretation on reliquefaction of saturated granular soils under cyclic loading. *Journal of Geotechnical and Geoenvironmental Engineering*, 127(5), 416–423. http://doi.org/10.1061/(ASCE)1090-0241(2001)127:5(416)

Oda, M., Koishikawa, I., & Higuchi, T. (1978). Experimental study of anisotropic shear strength of sand by plane strain test. *Soils and Foundations*, 25–38.

Uemura, K. (2010). *Effects of soil sample disturbance on liquefaction-induced strain development*. Master's dissertation, Hiroshima University, Hiroshima, Japan, 87 pp. (in Japanese).

Yasuda, S., Harada, K., Ishikawa, K., & Kanemaru, Y. (2012). Characteristics of liquefaction in Tokyo Bay area by the 2011 Great East Japan Earthquake. *Soils and Foundations*, 52(5), 793–810. http://doi.org/10.1016/j.sandf.2012.11.004

Yasuda, S., & Tohno, I. (1988). Sites of reliquefaction caused by the 1983 Nihonkai-chubu Earthquake. *Soils and Foundations*, 28(2), 61–72. https://doi.org/10.3208/sandf1972.28.2_61